Dual-beam Fourier domain optical Doppler tomography of zebrafish

Nicusor V. Iftimia, Daniel X. Hammer, R. Daniel Ferguson, Mircea Mujat, Danthu Vu, Anthony A. Ferrante

Physical Sciences Inc., 20 New England Business Center, Andover MA 01810
iftimia@psicorp.com

Abstract: We have developed a dual-beam Fourier domain optical Doppler tomography (FD-ODT) system to image zebrafish (*Danio rerio*) larvae. Two beams incident on the zebrafish with a fixed angular separation allow absolute blood flow velocity measurement to be made regardless of vessel orientation in a sagittal plane along which the heart and most of the major vasculature lie. Two spectrometers simultaneously acquire spectra from two interferometers with a typical (maximum) line rate of 18 (28) kHz. The system was calibrated using diluted milk and microspheres and a 0.5-mm thick flow cell. The average deviation from the set velocity from 1.4 to 34.6 mm/s was 4.1%. Three-dimensional structural raster videos were acquired of an entire fish, and through the head, heart, and upper tail of the fish. Coarse features that were resolved include the telencephalon, retina, both heart chambers (atrium and ventricle), branchial arches, and notochord. Other fine structures within these organs were also resolved. Zebrafish are an important tool for high-throughput screening of new pharmacological agents. The ability to generate high-resolution three-dimensional structural videos and accurately measure absolute flow rates in major vessels with FD-ODT provides researchers with additional metrics by which the efficacy of new drugs can be assessed.

©2008 Optical Society of America

OCIS codes: (170.0170) Medical optics and biotechnology; (170.4500) Optical coherence tomography; (170.3880) Medical and biological imaging.

References and links

1. B. R. White, M. C. Pierce, N. Nassif, B. Cense, B. H. Park, G. J. Tearney, B. E. Bouma, T. C. Chen, and J. F. de Boer, "In vivo dynamic human retinal blood flow imaging using ultra-high-speed spectral domain optical Doppler tomography," Opt. Express **11,** 3490-3497 (2003), http://www.opticsinfobase.org/abstract.cfm?URI=oe-11-25-3490.
2. D. Piao and Q. Zhu, "Quantifying Doppler Angle and Mapping Flow Velocity by a Combination of Doppler-Shift and Doppler-Bandwidth Measurements in Optical Doppler Tomography," Appl. Opt. **42,** 5158 (2003).
3. S. G. Proskurin, Y. He, and R. K. Wang, "Determination of flow velocity vector based on Doppler shift and spectrum broadening with optical coherence tomography," Opt. Lett. **28,** 1227-1229 (2000).
4. D. P. Davé and T. E. Milner, "Doppler-angle measurement in highly scattering media," Opt. Lett. **25,** 1523-1525 (2000).
5. A. Røyset, T. Støren, F. Stabo-Eeg, and T. Lindmo, "Quantitative measurements of flow velocity and direction using transversal Doppler optical coherence tomography," Proc. SPIE **6079,** 607925 (2006).
6. C. J. Pedersen, D. Huang, M. A. Shure, and A. M. Rollins, "Measurement of absolute flow velocity vector using dual-angle, delay-encoded Doppler optical coherence tomography," Opt. Lett. **32,** 506-508 (2007).
7. N. V. Iftimia, B. E. Bouma and G. J. Tearney, "Speckle reduction in optical coherence tomography by path length encoded angular compounding," J. Biomed. Opt. **8,** 260-263 (2003).
8. A. Mariampillai, B. A. Standish, N. R. Munce, C. Randall, G. Liu, J. Y. Jiang, A. E. Cable, I. A. Vitkin, and V. X. D. Yang, "Doppler optical cardiogram gated 2D color flow imaging at 1000 fps and 4D in vivo visualization of embryonic heart at 45 fps on a swept source OCT system," Opt. Express **15**, 1627-1638 (2007), http://www.opticsinfobase.org/abstract.cfm?URI=oe-15-4-1627.
9. M. W. Jenkins, D. C. Adler, M. Gargesha, R. Huber, F. Rothenberg, J. Belding, M. Watanabe, D. L. Wilson, J. G. Fujimoto, and A. M. Rollins, "Ultrahigh-speed optical coherence tomography imaging and visualization of the embryonic avian heart using a buffered Fourier Domain Mode Locked laser," Opt. Express **15**, 6251-6267 (2007), http://www.opticsinfobase.org/abstract.cfm?URI=oe-15-10-6251.

#96889 - $15.00 USD Received 2 Jun 2008; revised 4 Aug 2008; accepted 4 Aug 2008; published 20 Aug 2008
(C) 2008 OSA

10. Y. H. Zhao, Z. P. Chen, C. Saxer, S. H. Xiang, J. F. de Boer, and J. S. Nelson, "Phase-resolved optical coherence tomography and optical Doppler tomography for imaging blood flow in human skin with fast scanning speed and high velocity sensitivity," Opt. Lett. **25,** 114-116 (2000).
11. B. Park, M. C. Pierce, B. Cense, S. Yun, M. Mujat, G. Tearney, B. Bouma, and J. de Boer, "Real-time fiber-based multi-functional spectral-domain optical coherence tomography at 1.3 µm," Opt. Express **13**, 3931-3944 (2005), http://www.opticsinfobase.org/abstract.cfm?URI=oe-13-11-3931.
12. T. E. Ustun, N. V. Iftimia, R. D. Ferguson, and D. X. Hammer, "Real-time processing for Fourier domain optical coherence tomography using a field programmable gate array," Rev. Sci. Instrum., submitted.
13. N. V. Iftimia, D. X. Hammer, C. E. Bigelow, D. I. Rosen, T. E. Ustun, A. A. Ferrante, D. Vu, and R. D. Ferguson, "Toward noninvasive measurement of blood hematocrit using spectral domain low coherence interferometry and retinal tracking," Opt. Express **14,** 3377-3388 (2006), http://www.opticsinfobase.org/abstract.cfm?URI=oe-14-8-3377.
14. M. Mujat, B. H. Park, B. Cense, T. C. Chen, and J. F. de Boer, "Auto-calibration of spectral-domain optical coherence tomography spectrometers for in-vivo quantitative retinal nerve fiber layer birefringence determination," J. Biomed. Opt. **12,** 041205 (2007).
15. A. Nasevicius, and S.C Ekker, "Effective targeted gene 'knockdown' in zebrafish," Nature Genetics **26,** 216-220 (2000).
16. P. Goldsmith, "Zebrafish as a pharmacological tool: the how, why, and when," Current Opinion in Pharmacology **4,** 504-512 (2004).
17. D. J. Milan, T. A. Peterson, J. N. Ruskin, R. T. Peterson, and C. A. MacRae, "Drugs that induce repolarization abnormalities cause bradycardia in zebrafish," Circulation,**107,** 1355-1358 (2003).
18. R. Kopp, T. Schwerte, and B. Pelster, "Cardiac performance in the zebrafish *breakdance* mutant" J. Exp. Biol. **208,** 2123-2134 (2005).
19. D. X. Hammer, N. V. Iftimia, M. Mujat, R. D. Ferguson, D. Vu, A. A. Ferrante, and R. T. Peterson, "Blood flow and cardiac output measurements in zebrafish (Danio rerio) using dual-beam Fourier domain optical Doppler tomography," Circulation: Cardiovascular Imaging, submitted.

1. Introduction

Fourier domain optical coherence tomography (FDOCT) is well suited for Doppler flowmetry [1]. In contrast to a conventional time domain OCT configuration, the complex spectrum, and hence the phase, is completely accessible for post-processing without any changes or additions to the system hardware. Moreover, the depth profile is acquired without moving parts, which results in improved phase stability and a decrease in the minimum detectable velocity threshold. Also, short integration times increase the maximum detectable velocity threshold (before phase wrapping), further extending the flow measurement dynamic range.

Low coherence techniques detect singly back-scattered light within the range gate of the interferometer and are sensitive only to the flow velocity vector parallel to the incident beam. Thus, the angle between the incident beam and the flow field must be precisely known before absolute velocity measurements can be calculated. If the angle between the beam and the flow field is unknown in all three dimensions, three separate measurements at different angles are required to fully resolve the absolute velocity.

Several techniques have been developed to address this problem. Measurement of Doppler broadening indirectly yields flow speed but not vector direction [2,3]. Several other techniques have been demonstrated with the common characteristic that they separate the detected light into separate channels depending upon incident angle. Davé and Milner used a Wollaston prism and polarization optics to encode two incident beams into orthogonal polarization components [4]. Røyset et al. used a free-space interferometer and a quadrant detector to encode angle [5]. Pedersen et al. [6] recently demonstrated an approach to retrieve the full velocity vector using a technique for pathlength encoding that was first introduced by Iftimia et al. [7] for speckle averaging. Pathlength encoding uses a glass plate inserted into a portion of the incident beam to split the beam into two sub-beams with distinct incident angle and group delay. One consequence of the pathlength encoding technique is that the overall depth range is reduced by one half since it is split between the two channels. This trade-off can be more significant for spectrometer-based Fourier domain methods because of their limited range compared to time domain methods.

In this paper we describe our extension of this approach with Fourier domain methodology and using two distinct channels for full range detection. We have developed a dual-beam approach that separates the light at the source into two interferometers, which share the same

#96889 - $15.00 USD Received 2 Jun 2008; revised 4 Aug 2008; accepted 4 Aug 2008; published 20 Aug 2008
(C) 2008 OSA

sample and reference optical paths. Like the pathlength encoding technique, the dual-beam approach only removes angular ambiguity in one plane. However, for many biological applications where absolute velocity calculation is necessary to achieve a quantitative measure of function, major flow is already confined to one plane. For example, in the zebrafish (*Danio rerio*) larva (Fig. 1), there is little deviation in the flow angle for the heart and major vessels with respect to the sagittal plane bisecting the center of the animal.

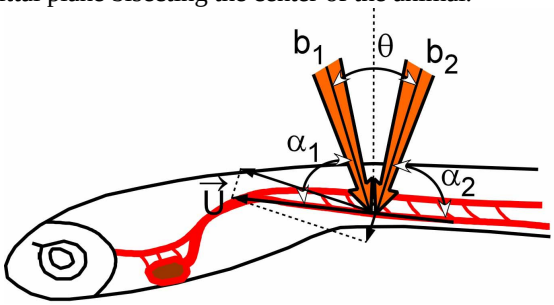

Fig. 1. Dual-beam approach for measurements on zebrafish (side view). All vectors and angles are in a sagittal plane bisecting the fish at the location of the dorsal aorta.

The angles between the beamlets and the flow field (α_1 and α_2) can be found from measurement of the velocity in both channels (b_1 and b_2) according to [6]:

$$\alpha_1 = \tan^{-1}\left(\cot(\theta) - \frac{b_2}{b_1 \sin(\theta)}\right), \quad \alpha_2 = \pi - \theta - \alpha_1 .$$

The magnitude of the velocity vector U is then given by:

$$U = \frac{b_1}{\cos \alpha_1} = \frac{b_2}{\cos \alpha_2} .$$

There have been several recent reports on the application of high-speed FDOCT and FD-ODT techniques to the study of developmental biology in general and congenital heart disease in particular [8,9]. The zebrafish is an emerging model for drug discovery in high-throughput screening applications because it has several advantages over other models, including small size (to fit in rapid screening microwell plates), optical transparency, and genetic similarities to humans. High throughput screening with the use of functional cardiac and blood flow metrics (cardiac output, ejection fraction, etc.) require absolute comparison when agents are applied systemically to a large batch of animals. Furthermore, the zebrafish anatomy is well suited to the dual beam setup because flow in the major organs and arteries can be easily aligned to the plane in which the illumination beams lie.

This paper describes the dual-beam FD-ODT system and its application to zebrafish imaging. System characterization, structural imaging, and preliminary cardiac blood flow measurements were performed. The overall aim of the research is the development of high-throughput assays for drug discovery using zebrafish.

2. Dual-beam Doppler system description

2.1 Optical setup

The schematic of the dual-beam FD-ODT system is shown in Fig. 2. The illumination source is a Broadlighter with dual superluminescent diodes (Superlum Diodes Ltd., Russia). The output is split between two fiber-based interferometers that probe the specimen in the sample path with two beams at different incident angles. A fixed optical pathlength difference is set between the two interferometers in both the reference and sample paths to avoid cross-talk. Because the individual channels are separate, the dual-beam setup does not degrade the quality of the OCT intensity image.

#96889 - $15.00 USD Received 2 Jun 2008; revised 4 Aug 2008; accepted 4 Aug 2008; published 20 Aug 2008
(C) 2008 OSA

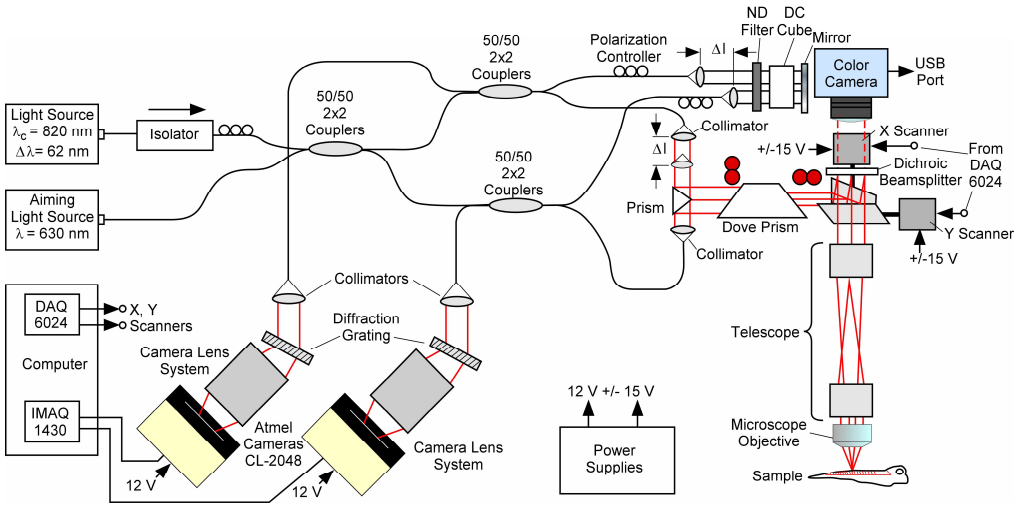

Fig. 2. Schematic of the dual-beam system.

Both reference paths use a single optical delay line comprised of a mirror, neutral density filter, and dispersion compensation cubes. The mirror is mounted to a linear stage for coupled (channel) range gate adjustment. In the sample path, the pathlength difference between the two channels is adjusted independently without affecting focus by translation of the stage upon which one of the fiber collimators is mounted. This adjustment is important to insure that the sample images from the two channels are precisely overlapped in depth for absolute velocity measurement. The sample arms are combined together with a reflective prism into the front-end optics. A dove prism mounted in a rotary mount is used to rotate the beams around the optical axis of the telescope and objective.

The front-end optics are configured in a conventional scanning confocal arrangement. Two mirrors mounted to a pair of galvanometers (Cambridge Technologies Inc., Cambridge MA) are used for lateral scanning. Two telescope objectives each composed of an off-the-shelf achromat and a custom meniscus lens (for better field flatness) expand the beam into a 10×, 0.25 NA microscope objective (Leica, Wetzlar, Germany) with a diameter of 10 mm, an effective focal length of 20 mm, and a working distance of 12 mm. As long as the two beams are properly collimated into the telescope, they will overlap at the focus since they pass through the same optical elements. This is true even if they are not symmetric in their displacement about the optical axis, although this displacement will affect the incident angles of each beam and any angular asymmetry between them. The angle between the beams is set by the spacing between the beams and the f/# of the microscope objective. Larger angles will produce larger phase changes for a fixed flow velocity but can only be achieved with a shorter focal length objective (lower f/#), and hence a shorter depth of focus. Therefore, the angle was chosen as a trade-off between phase change and depth of focus.

The zebrafish is also imaged through the same optical path with a USB color CCD camera (BlueFox, Matrix Vision, Oppenweiler, Germany). Room light illuminates the entire CCD field. A low-pass dichroic beamsplitter passes visible light into the camera objective and reflects near infrared light back-scattered from the specimen into the galvanometers and back into the interferometers. A visible aiming laser is used to visualize the OCT scan on the CCD. The entire front end optical hardware, from collimator to microscope objective, and including the USB camera, are all mounted on a large plate attached to a linear translation stage that controls the system focus with respect to the sample. Thus, the beam focus could be moved through structures in the zebrafish larvae with this stage. During system alignment, optimal OCT signal-to-noise (and lateral resolution) was achieved by aligning both the focus and the range gates close to the zero fringe point.

#96889 - $15.00 USD Received 2 Jun 2008; revised 4 Aug 2008; accepted 4 Aug 2008; published 20 Aug 2008
(C) 2008 OSA

The interferometer detector paths consist of two identical spectrometers comprised of a collimator, holographic transmission grating with 1200 lines/mm (Wasatch Photonics Inc., Logan UT), and custom-designed, multi-element objective. The objective was designed to control field flatness, spherical and chromatic aberration and can accommodate a bandwidth up to 200 nm. The dispersed spectra are imaged onto 10-μm, 2048-pixel CCD linear array detectors (e2v Technologies/Atmel Inc., Essex England). The signals from both cameras are digitized with a dual-channel CameraLink framegrabber (National Instruments Inc., Austin TX). A data acquisition (DAQ) board (National Instruments Inc., Austin TX) is used to generate all analog waveforms to drive the lateral scanning galvanometers and digital timing signals for synchronization between the galvanometers, linear detectors, and framegrabber. Photographs of the dual-beam FD-ODT system with primary components labeled are shown in Fig. 3.

Several factors were considered when configuring the image scan parameters for the zebrafish. First, to extract phase changes from adjacent A-lines [1,10], it is necessary to insure that there is proper beam overlap. The general rule of thumb is to maintain a spacing of one-tenth the spot size between adjacent A-lines for generation of phase maps uncorrupted by phase noise associated with scanner motion [11]. For the measured spot size of ~12 μm (see Section 3 below), sufficient beam overlap was achieved if the lateral pixel size was set to ~1 μm, for example a 1-mm scan comprising 1024-pixels. The condition was met for all images and videos where blood flow measurements were made.

The second consideration was the integration time and scan type. Since the primary target for the phase measurement was the heart with flow velocities exceeding 25 mm/s, the instrument was configured for image acquisition with the shortest integration time possible while still maintaining good signal-to-noise ratio. Raster scans were used primarily for obtaining 3-D structural information, however there was no guarantee that the cardiac cycle was not in its quiescent phase when the beam was positioned over regions that have

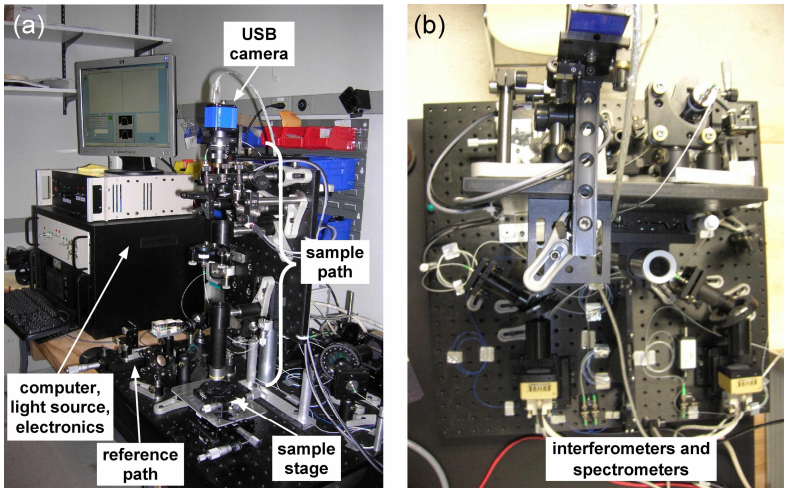

Fig. 3. Photograph of the dual-beam system. (a) Side view. (b) Top view.

significant flow. This issue is compounded by small vessel sizes: the inner lumen of the ventral aorta where cardiac output measurements were made was typically <30 μm in diameter, and all other vessels were even smaller and more difficult to locate. To detect flow during all phases of the cardiac cycle, a slice positioned through the exact plane of flow was acquired with repeated stationary frame scans (i.e., B-scans). As long as the beams were positioned in the plane of flow in the vessel of interest, B-scans could be collected either in a plane parallel to the vessel (sagittal section) or perpendicular to the vessel (axial section). At 18 fps, 100 B-scans collected ~10-14 cardiac cycles for the typical heart rate of 125-150 beats per minute (bpm) for zebrafish larvae that are <1 week old. This allowed a temporal

#96889 - $15.00 USD Received 2 Jun 2008; revised 4 Aug 2008; accepted 4 Aug 2008; published 20 Aug 2008
(C) 2008 OSA

resolution of 1 to 3 frames during systole when most flow occurred. This imaging protocol design also allowed cardiac phase-binned composite images to be generated for each phase of the entire cardiac cycle to reduce OCT speckle noise.

2.2 Acquisition and analysis software

Specialized acquisition and analysis software was developed for the dual-beam FD-ODT system. The front panel of the acquisition software is shown in Fig. 4. The acquisition software displays the processed intensity images from both channels as well as from the CCD camera. It also controls all analog and digital waveform generation and routing to and from the DAQ and framegrabber. Single processed images can be saved in a variety of formats and raw spectral data is packed into a binary file and saved with the CCD video file using time-stamped filenames. The maximum acquisition line rate for the linear detector is 28 kHz, but generally videos were acquired at 18.4 kHz (18 fps × 1024 A-lines).

The acquisition software was designed to collect conventional raster and line scans for structural and blood flow imaging as described above. It was also configured to acquire a custom raster scan to aid in beam alignment over the heart and vessel and visualization of flow. Each line of the custom raster scan was composed of multiple stationary lines to allow for imaging in one plane of the entire cardiac cycle. Therefore, the frame rate and number of lines were adjusted depending upon the heart rate of each subject.

In both acquisition and analysis software, the digitized spectra from the linear detectors are processed with background subtraction, high-pass filtering, λ-k interpolation, dispersion compensation, fast Fourier transformation (FFT), and logarithmic scaling in the usual manner [12]. An iterative numerical dispersion compensation algorithm is used in addition to the fixed hardware dispersion cubes in the interferometer reference paths for precise optimization of dispersion mismatch arising from system and sample optical properties [13]. With full FDOCT processing, the display rate was only 1-2 fps. Future upgrades include use of a dedicated real-time FDOCT processing board for display at the acquired frame rates [12].

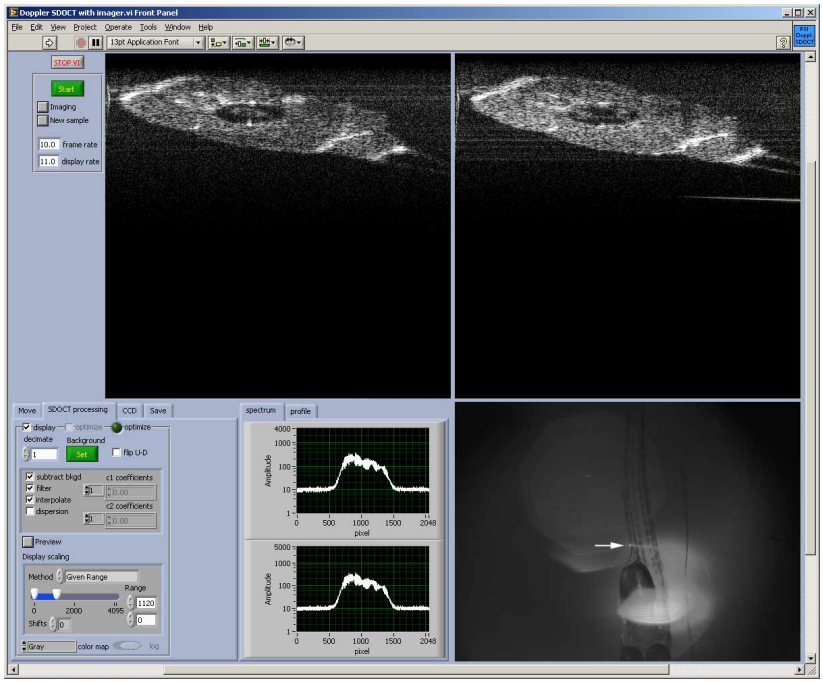

Fig. 4. Front panel of the acquisition software. OCT B-scan is across the tail just below the swim bladder. Arrow in the CCD image indicates position of the OCT line. (Aspect ratio of the scan is not 1.)

#96889 - $15.00 USD Received 2 Jun 2008; revised 4 Aug 2008; accepted 4 Aug 2008; published 20 Aug 2008
(C) 2008 OSA

The analysis software processes the spectral data to generate OCT intensity and phase images for both channels and an absolute velocity image from the two phase images. The processing to generate phase images is similar to that previously reported [1], including correction for phase artifacts due to bulk motion, except that the algorithm handles fixed phase noise differently. First, offsets from line to line are removed with a slightly different technique. Second, phase variations in low signal regions are removed by using an intensity-dependent threshold. Third, the pixel-to-pixel fixed pattern phase noise is removed by subtracting an image summed from frames acquired during the quiescent phase of the cardiac cycle from all other cardiac phases where flow exists. This resulted in phase maps that were substantially free of non-flow phase artifacts. For videos acquired where low flow or non-pulsatile flow was dominant, and where the quiescent phase is impossible to distinguish, the fixed pattern phase noise was not subtracted. Phase averaging was generally used in the low flow case to extract a quantitative measurement of flow velocities close to the detection limit.

For the dual-beam system, generation of accurate absolute velocity maps requires that the images from the two channels overlap precisely. The analysis software was set up to allow the images to be shifted in both axes with respect to one another if there were small errors in axial alignment. Also, for acquisition of sagittal sections (i.e., scanned along a vessel), one additional processing step is applied to remove the shear between channels in both the intensity and phase images. For axial sections (i.e., scanned across the vessel), it is not possible to remove the shear, and therefore axial alignment of the focus and range gate positions between the two channels are critical in this scan configuration. OCT signals provide only coarse confirmation of this alignment. It was easier to confirm axial alignment and focus by comparison of anatomical features between the two channels in the region of interest. Any disparity between the images indicated that the beams crossed at different axial locations. This was remedied by adjustment of system focus.

Once the phase images are generated, the absolute velocity is found from the phase maps using the equations presented in Section 1 with knowledge of the angle between the beams. Other post-processing software features include image transpose, flattening, alignment (for generation of composite images), and generation of additive and difference images, the latter of which was particularly useful to verify precise channel overlap. Generation of uncompressed and compressed videos and images with multiple panels (e.g., an intensity and phase montage) and color-coded, partially transparent, absolute blood flow overlays onto the intensity frame are also possible.

2.3 Zebrafish preparation

All zebrafish were imaged between 5 and 8 days post fertilization (dpf). Because the instrument was configured to image through the dorsal surface while a ventral view of the larvae proved to be optimal to access the heart and primary vessels of interest, the animals were embedded in low gel temperature agarose for imaging. The larvae were lightly anesthetized in 50 μg/ml Tricaine and then transferred in a small droplet of liquid to the center of a small Petri dish. Low gelling temperature agarose was cooled to 37ºC, supplemented with 50 μg/ml Tricaine, and 1 ml was carefully added to the droplet containing the larva. After the gel set, another 1-5 ml of 50 μg/ml Tricaine solution was added to the dish to keep the gel from drying. The animals remained healthy for periods up to several hours with no signs of stress. For experiments aimed at measuring decreased cardiac output, additional Tricaine was added incrementally from a 4 mg/ml stock solution.

3. Results

3.1 System Calibration and Performance

For accurate absolute velocity measurement, the dual-beam approach obviates the need for *a priori* knowledge of the angle between the flowing target and each imaging beam (in one plane): knowledge of the angle between the two imaging beams is sufficient. The angle between the two beams, as well as the spot size and depth of focus, which indicate the optical

#96889 - $15.00 USD Received 2 Jun 2008; revised 4 Aug 2008; accepted 4 Aug 2008; published 20 Aug 2008
(C) 2008 OSA

performance of the microscope, can be easily determined during system calibration with a set of knife-edge measurements. The results for the knife edge measurements are shown in Fig. 5. The measured (fit) spot diameter for the beams shown in Fig. 5(a) was 13.8 (9.3) and 11.2 (9.2) µm, and the measured depth of focus was 87.2 and 105.2 µm.

One of the consequences of the relatively narrow depth of focus of the system was that useful information could not be collected from the entire thickness of the zebrafish. For example, in the structural images, the signal outside of the $1/e^2$ points drops precipitously (see Fig. 8(b) below). However, the depth of the entire thoracic cavity was only ~100 µm and therefore the heart flow measurements were not affected. The angle between beams, shown in Fig. 5(b), was 14.5°. The small difference between beam angles (6.96° and 7.55°) also indicates good symmetry of beam displacement about the optical axis. The theoretical diffraction-limited spot diameter for the 10× microscope objective (f/5 focusing for a 4-mm input beam diameter) is 10 µm indicating good optical performance ($M^2 \approx 1.2$) and alignment.

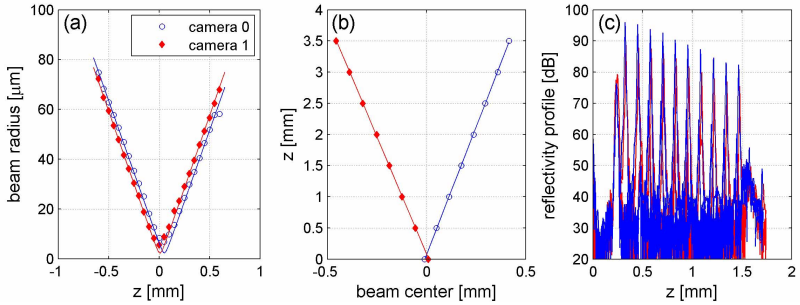

Fig. 5. System calibration. (a) Knife-edge measurements through the beam waists. One channel is shifted laterally for better visualization. (b) Lateral position of beam center in the axial dimension measured with knife-edge. (c) Depth attenuation measured with reflector.

Depth-dependent attenuation in the spectrometer signal is an inherent limitation of FDOCT systems and arises from the fixed detector pixel size. Essentially, the fringe contrast is reduced as a function of frequency (i.e., as a function of depth in the Fourier transformed cross-sectional profile). For the FDOCT spectrometer, this depth decay can be used as a metric of the quality of the spectrometer optics. It can also be used to indicate proper alignment because a misaligned beam will lead to broadening of the focused line and hence a further reduction in fringe contrast. The depth-dependent attenuation is measured by placing a highly reflective target (e.g., cover slip or mirror) in the sample path and recording the profile along the axial depth. The depth-dependent decay profiles for both spectrometers are shown in Fig. 5(c). (The fixed peak near 0.2 mm is in the reference path and is used to calculate an interpolation array used in FDOCT image processing [14].) The depth range in air is 1.73 mm corresponding to a range in tissue of 1.25 mm. The total attenuation over a 1.5 mm range was ~14 dB for both cameras. Measurement of the width of a single peak also gives a measure of the coherence length and axial resolution. The measured coherence length (at 6 dB intensity) was 5.4 µm which can be compared to the theoretical resolution for this source (λ_c = 820 nm, $\Delta\lambda$ = 62 nm) of 4.8 µm in air.

The absolute velocity measurement and velocity dynamic range were verified using 200- and 500-µm thick flow cells (Starna Cells Inc., Atascadero CA) and a calibrated pump. The cells were 8-mm wide and 40-mm long (from inlet to outlet). All scans were collected at least 1 mm from the cell wall and several millimeters from the inlet and outlet to avoid turbulent or irregular flow. Diluted milk or 2- and 8-µm microspheres were flowed through the cells with velocities from 0 to 69 mm/s. Flow with scanning and stationary beams (i.e., across and along the flow field or from a fixed location) produced similar results although generally the measurements with scanning beams exhibited increased phase instability and noise arising from the moving galvanometers.

Figure 6 shows the results from a measurement with a stationary beam. Figure 6(a) shows absolute velocity profiles of milk flowing in the 500-µm cell for a range of velocities. The

#96889 - $15.00 USD Received 2 Jun 2008; revised 4 Aug 2008; accepted 4 Aug 2008; published 20 Aug 2008
(C) 2008 OSA

average depth profiles across all 1024 A-lines in the image (i.e., temporal averages) are shown in Fig. 6(b), indicating laminar and parabolic flow. Figure 6(c) plots the measured velocity as a function of set velocity. The average error (i.e., deviation from the set velocity) for flows from 1.4 to 34.6 mm/s was 4.1%. For the acquisition line rate of 18.43 kHz (18 frames per second, fps, for a 1024 A-line frame), the peak velocity before wrapping for the dual-beam system is 46 mm/s, corresponding to an average velocity (assuming parabolic flow) of 30.6 mm/s. Wrapping is detected above ~30 mm/s in Fig. 6(c) and is clearly evident in the lower right panel in Fig. 6(a), where the maximum flow changes color.

When the signal-to-noise ratio (SNR) is high (as is the case for the zebrafish images), the minimum detectable velocity is limited by phase noise. In the limit of high line rates (short integration times) where SNR is diminished, amplitude noise can begin to dominate and become the limiting factor. A measurement of phase stability in the absence of flow [1] indicates that the minimum detectable velocity is ~109 μm/s. Using a stationary mirror in the sample arm we measured the phase differences between consecutive A-lines. The standard deviation of the phase differences (σ), which quantifies the phase stability, gives the minimum detectable Doppler frequency shift ($f\sigma / 2\pi$, where f is the A-line frequency) and therefore the minimum detectable velocity. Flow <1 mm/s was resolved, although the peristaltic pump produced unstable flow at low velocities and prevented verification of velocities closer to the minimum detectable threshold.

There were small peaks at the vessel walls (Fig. 6(b)) associated with boundary artifacts and a slight difference (~2%) in the measured length of the cell. The latter was associated with small differences in spectrometer alignment (e.g., tilt of grating) that caused disparities in the wavelength spread on the linear detectors.

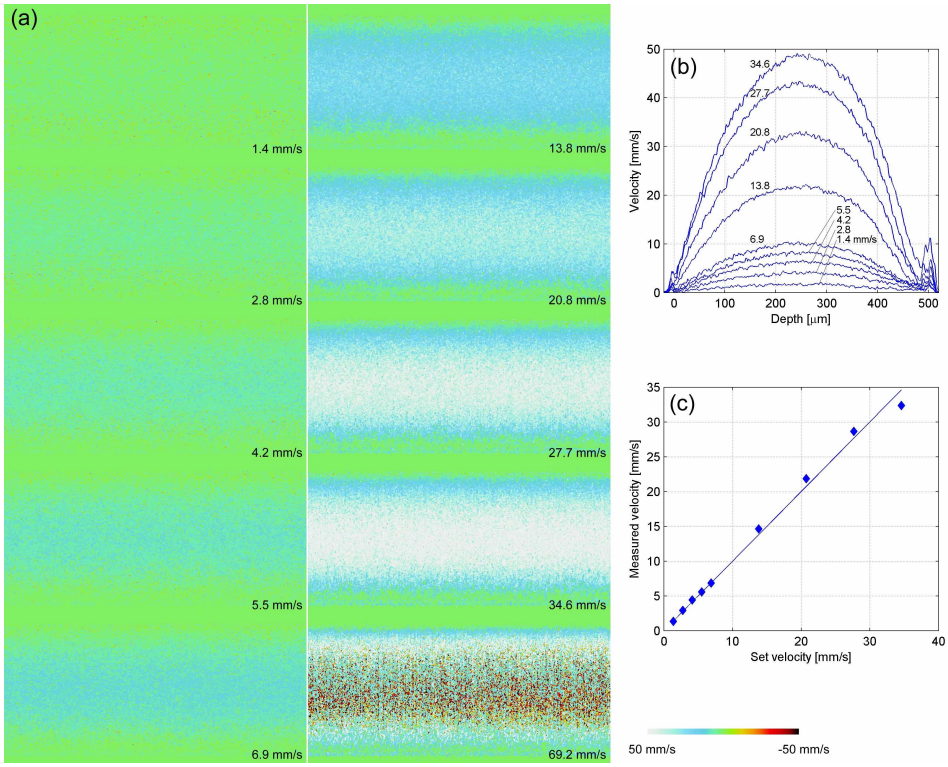

Fig. 6. Doppler flow calibration using diluted milk in a 0.5-mm deep flow cell. (a) Absolute velocity profiles of flow in the cell. (b) Average depth profiles across the image. Parabolic flow is clearly evident. (c) Comparison of set velocity to measured average velocity. Phase wrapping occurred above ~30 mm/s and is clearly visible at 69.2 mm/s. The beams were not scanned and were placed ≥1 mm from the cell wall.

#96889 - $15.00 USD Received 2 Jun 2008; revised 4 Aug 2008; accepted 4 Aug 2008; published 20 Aug 2008
(C) 2008 OSA

3.2 Zebrafish structural imaging

Structural images and accompanying video of the zebrafish are shown in Figs. 7-10. All videos present a ventral view and fly-through in the left panel and either a sagittal or an axial view and fly-through in the right panel. In all views, the pixels were made square and, when necessary, one view was resized in the horizontal dimension to match that of the other view.

Figure 7 shows a scan of the entire fish oriented with dorsal side up. The ventral view (Fig. 7(a)) is a section at the level of the viscerocranium and swim bladder and the axial view (Fig. 7(b)) is a section through the heart between the atrium and ventricle. Gross anatomical features such as the eyes, endoskeleton, otic capsule, heart, pectoral fin, swim bladder, stomach, and notochord can be easily identified.

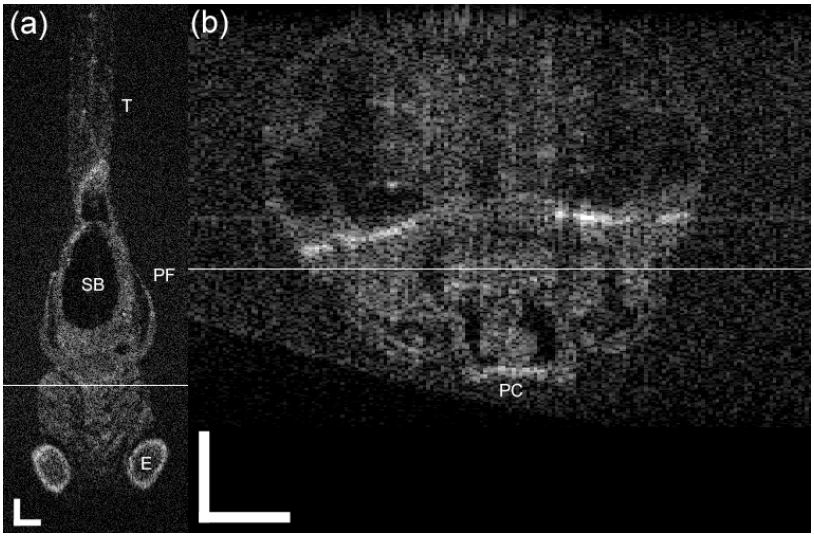

Fig. 7. (Media 1) Fly-through video of the entire fish. (a) Ventral view (left panel of video). (b) Axial view (right panel of video). The horizontal line in (a) indicates the cross-section in (b) and the horizontal line in (b) indicates the cross-section in (a). Scale bar = 100 μm. T: tail, SB: swim bladder, PF: pectoral fin, E: eye, PC: pericardial cavity. The raw video was acquired at 60 fps.

Figure 8 shows a scan through the upper body and head of a zebrafish oriented ventral side up. The ventral view (Fig. 8(a)) is a section through the center of the eye and otic capsule and the axial view (Fig. 7(b)) is a section near the midline of the fish. In the ventral view from front to back are labeled the mouth, retina, otic capsule, and the top of the swim bladder. Because of the limited depth of focus and FDOCT depth attenuation, structures in the brain are not well resolved, although in some of the slices the telencephalon is visible. The ventral slices through the heart show contractions of the beating atrium and ventricle. Note that distinct retinal layers can be seen in the eyes.

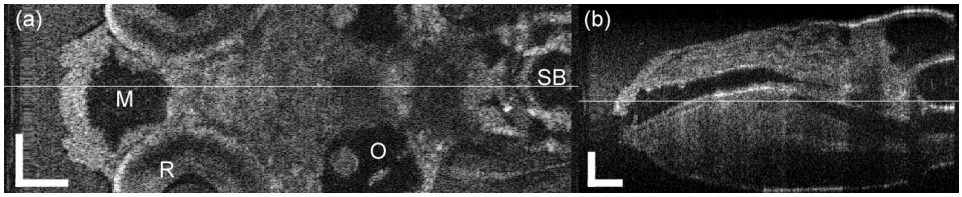

Fig. 8. (Media 2) Fly-through video of the head and upper body of fish. (a) Ventral view. (b) Sagittal view. Scale bar = 100 μm. The raw video was acquired at 15 fps. M: mouth, R: retina, O: otic capsule, SB: swim bladder.

#96889 - $15.00 USD Received 2 Jun 2008; revised 4 Aug 2008; accepted 4 Aug 2008; published 20 Aug 2008
(C) 2008 OSA

Figure 9 shows a scan through the thoracic (pericardial) cavity. The two chambers of the heart are clearly visible in both ventral and axial fly-throughs. Because the zebrafish was heavily anesthetized when this raster scan was acquired, there is little motion in the heart.

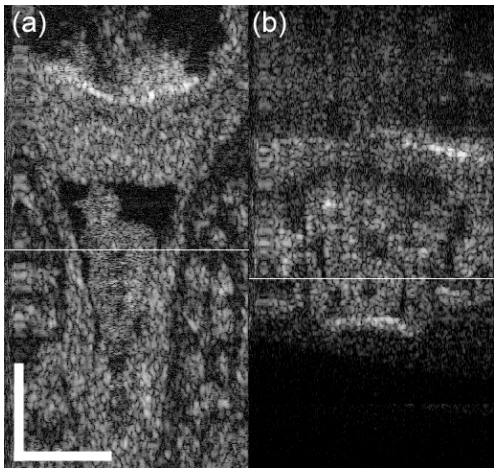

Fig. 9. (Media 3) Fly-through video of the heart. (a) Ventral view. (b) Axial view. Scale bar = 100 μm. The raw video was acquired at 72 fps.

Figure 10 shows a scan through the upper trunk of the fish. The notochord is clearly visible in both ventral and axial views. The junctions between the segments of the notochord are <10 μm and are clearly resolved in the high resolution FDOCT images. The dorsal aorta (DA) and the posterior cardinal vein (PCV) are resolved in other ventral slices.

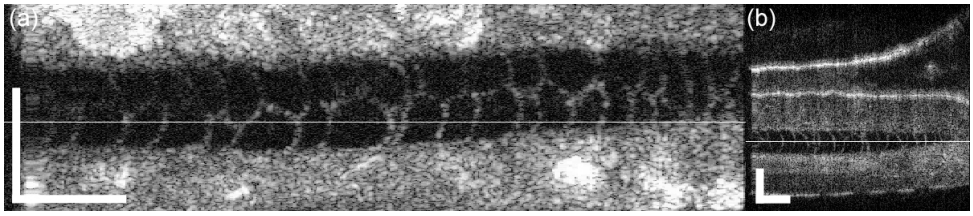

Fig. 10. (Media 4) Fly-through video of the notochord. (a) Ventral view. (b) Sagittal view. Scale bar = 100 μm. The raw video was acquired at 10 fps.

3.3 Zebrafish Doppler imaging

Preliminary Doppler images of blood flow in the zebrafish heart were acquired. Axial and sagittal cross sectional videos through the heart are shown in Figs. 11 and 12. In the axial view in Fig. 11, the zebrafish is oriented at ~45 deg. with respect to the OCT scan. Each video frame is a composite generated from 10 cardiac cycles (HR = 117 bpm). Slight differences in the anatomy above and below the focus (at the heart) can be seen and are a result of the angle between the beams in this scanning orientation, as discussed above in Section 2. Pulsatile, turbulent flow in both chambers of the heart is visible as is flow in several vessels immediately adjacent to the heart.

The sagittal cross-sectional view is shown in Fig. 12, where only a single channel is presented. Each composite frame is generated from 13 cardiac cycles (HR = 158 bpm). Flow all along the ventral aorta (VA) is clearly visualized. Maximum flow in the VA (11-μm diameter measured from intensity image) is 32.4 mm/s (measured with velocity maps scaled to ±50 mm/s). From the HR, flow velocity, and vessel diameter, the cardiac output is calculated to be 31 nL/min. Further along the VA, the phase and velocity reversal indicate an abrupt change in the flow direction out of the sagittal plane (into the page). The absolute magnitude of the flow where it changes direction cannot be reliably determined. A more

#96889 - $15.00 USD Received 2 Jun 2008; revised 4 Aug 2008; accepted 4 Aug 2008; published 20 Aug 2008
(C) 2008 OSA

thorough analysis of blood flow velocity measurements and cardiac output calculations are presented elsewhere [19].

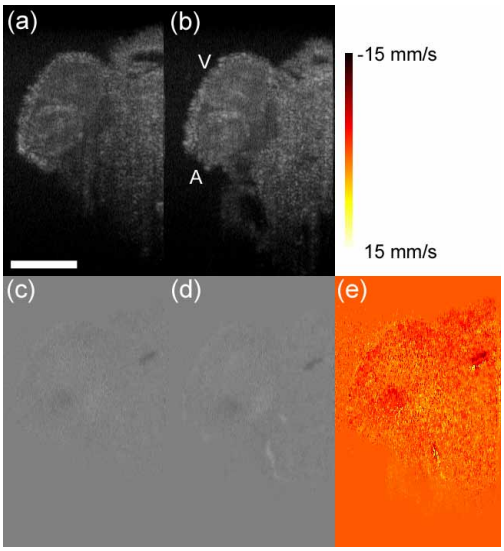

Fig. 11. (Media 5) Axial view of zebrafish heart. (a), (b) Channel 1 and 2 intensity images; (c), (d) Channel 1 and 2 phase map; (e) Absolute velocity map. Scale bar = 100 μm. A: atrium, V: ventrical.

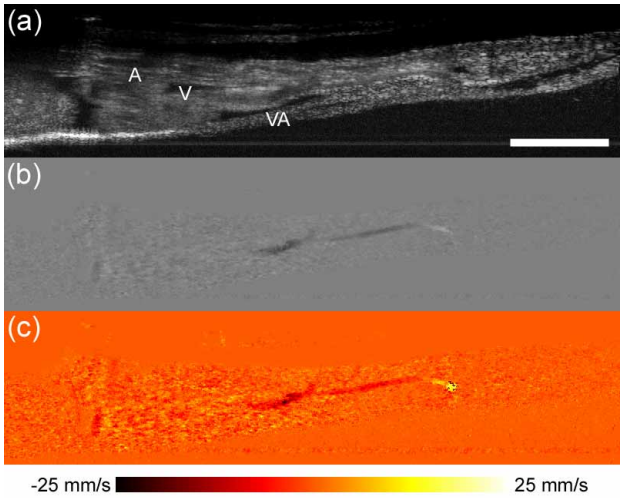

Fig. 12. (Media 6) Sagittal view of zebrafish heart. (a) Channel 1 intensity image, (b) Channel 1 phase image, (c) Absolute velocity map. Scale bar = 100 μm. VA: ventral aorta.

4. Discussion

Zebrafish have found increasing usage in the last few years for developmental biology and drug discovery for numerous reasons: they are genetically, anatomically, and pharmacologically similar to humans; their external development and optical transparency facilitate real time visualization of their organs; they are easy to genetically manipulate (knock-outs, etc.); and they readily take up small molecules [15]. Also, because of their rapid proliferation and small size, zebrafish represent a significant cost saving over rodents and other small animals in terms of husbandry and associated chemical (reagents, compounds, etc.) usage [16].

#96889 - $15.00 USD Received 2 Jun 2008; revised 4 Aug 2008; accepted 4 Aug 2008; published 20 Aug 2008
(C) 2008 OSA

Zebrafish are an excellent model for both cardiac drug discovery and cardiotoxicology. Drugs known to cause heart rhythm abnormalities in humans generally affect zebrafish larval cardiac function [16,17]. One impediment to wide spread adoption of zebrafish for cardiac assays is the lack of high-throughput techniques for simultaneous structural imaging and absolute blood velocity measurement. Current approaches for functional zebrafish imaging usually involve high-speed bright-field video microscopy [18]. This technique allows heart rate to be monitored in a high-throughput manner. Blood flow in smaller vessels (e.g., DA and PCV) can also be quantified. However, this technique requires high frame rates to make estimates of flow in the VA and doesn't provide depth sectioning capabilities. Thus no high-throughput imaging system has been developed that provides enough information to fully characterize the systemic effect of a particular drug. Optical coherence tomography provides micron level axial and lateral resolution, three-dimensional mapping of a sample. Fourier domain techniques provide additional advantages in terms of high speed and direct access to the phase of the signal.

We have developed a dual-beam Fourier domain optical Doppler tomography system for high-throughput screening of zebrafish. Knife-edge measurements indicate good optical performance ($M^2 \approx 1.2$) with no degradation in the OCT intensity image for the individual channels. Thus high speed, three-dimensional maps can be made of the fine structural characteristics of the zebrafish anatomy. The system has a wide dynamic range (~0.1 to 30 mm/s) that matches the range of flow velocities found in the heart and major vessels (VA and DA) of the young (< 8 dpf) zebrafish larvae. Absolute velocity measurements in a flow cell deviated by only 4% from the set velocity. The dual-beam setup provides absolute velocity measurement without critical determination of vessel angle in one plane. This is also suited to the zebrafish, whose heart and major trunk and tail vessels (DA and PCV) all lie within one sagittal plane. When flow deviates from this plane (as seen in the lower VA below the heart in Fig. 12), the absolute velocity cannot be determined with the dual beam setup. This limitation will require some level of coarse subject alignment to the instrument, but with high speed OCT intensity imaging and auxiliary CCD imaging, should not impede future development of automated techniques for high throughput operation.

This paper described the system performance, high resolution structural imaging, and preliminary cardiac Doppler flowmetry of zebrafish larvae. At the development stage for the measurement presented here, the length and diameter of the zebrafish heart was roughly 100 μm, or nearly 5 times smaller than avian or frog embryos previously measured with Fourier domain techniques [8,9]. Maximum flow in the VA of a 5 dpf zebrafish was measured at 32.4 mm/s yielding a cardiac output of 31 nL/min. We have also measured blood flow in other vessels (particularly the DA), performed further cardiac output calculations, and observed drug-induced changes in cardiac output [19]. Future efforts will automate the FD-ODT zebrafish cardiac assay system for true high-throughput data collection and analysis. The FD-OCT raster-scan confocal imaging system is also amenable to multi-photon fluorescence imaging applications.

It should be clear from the structural videos shown in Figs. 7-10 that there is significant value in full three-dimensional mapping of the zebrafish. Essentially, any organ or structure in the zebrafish can be studied from any vantage point during development, upon administration of pharmacological agents, or during any other induced changes. Figure 8 shows good resolution of the heart chambers, the eye, and the ventral portion of the brain. Other parts of the brain (e.g., telencephelon, optic tectum, cerebellum, meyelencephalon) could be better resolved by moving it within the system focus. Figures 9 and 10 illustrate high resolution 3-D imaging of the heart chambers and the notochord in the upper tail, respectively. This work demonstrates the potential of FD-ODT for full structural and functional characterization of the zebrafish.

Acknowledgments

This work was supported by NIH grant R43 HL086809. We thank Randy Peterson for helpful comments.

#96889 - $15.00 USD Received 2 Jun 2008; revised 4 Aug 2008; accepted 4 Aug 2008; published 20 Aug 2008
(C) 2008 OSA